

Identification of two distinct inactive conformations of the β_2 -adrenergic receptor reconciles structural and biochemical observations

Ron O. Dror^{a,1}, Daniel H. Arlow^{a,1}, David W. Borhani^a, Morten Ø. Jensen^a, Stefano Piana^a, and David E. Shaw^{a,b,2}

^aD. E. Shaw Research, New York, NY 10036; and ^bCenter for Computational Biology and Bioinformatics, Columbia University, New York, NY 10032

Edited by Axel T. Brunger, Stanford University, Stanford, CA, and approved January 28, 2009 (received for review November 6, 2008)

Fully understanding the mechanisms of signaling proteins such as G protein-coupled receptors (GPCRs) will require the characterization of their conformational states and the pathways connecting those states. The recent crystal structures of the β_2 - and β_1 -adrenergic receptors in a nominally inactive state constituted a major advance toward this goal, but also raised new questions. Although earlier biochemical observations had suggested that these receptors possessed a set of contacts between helices 3 and 6, known as the ionic lock, which was believed to form a molecular switch for receptor activation, the crystal structures lacked these contacts. The unexpectedly broken ionic lock has raised questions about the true conformation(s) of the inactive state and the role of the ionic lock in receptor activation and signaling. To address these questions, we performed microsecond-timescale molecular dynamics simulations of the β_2 -adrenergic receptor (β_2 AR) in multiple wild-type and mutant forms. In wild-type simulations, the ionic lock formed reproducibly, bringing the intracellular ends of helices 3 and 6 together to adopt a conformation similar to that found in inactive rhodopsin. Our results suggest that inactive β_2 AR exists in equilibrium between conformations with the lock formed and the lock broken, whether or not the cocrystallized ligand is present. These findings, along with the formation of several secondary structural elements in the β_2 AR loops during our simulations, may provide a more comprehensive picture of the inactive state of the β -adrenergic receptors, reconciling the crystal structures with biochemical studies.

GPCR | ionic lock | molecular dynamics

The recent crystal structures of the β_2 -adrenergic receptor (β_2 AR) represented a significant advance in the study of G protein-coupled receptors (GPCRs) (1–4), which constitute the largest class of both human membrane proteins and drug targets (5). β_2 AR, an important target for cardiac and asthma drugs, has long served as the prototypical ligand-binding GPCR and has been extensively characterized in experimental work over several decades (6).

The β_2 AR crystal structures are very similar to one another, yet β_2 AR function relies on its ability to adopt multiple conformations. A conformational change from an inactive state to an active state enables the receptor to transmit a signal from the extracellular ligand-binding site to an intracellular G protein, thereby initiating diverse intracellular signaling processes. Several studies have indicated that the active and inactive states of β_2 AR each comprise multiple receptor conformations with different implications for signaling (7, 8). In the present work, we used molecular dynamics (MD) simulations to characterize functionally important aspects of the inactive conformational ensemble.

We focused, in particular, on the implications of a surprising feature of the β_2 AR crystal structures: the absence of a salt bridge between the intracellular ends of helices 3 and 6 in the inactive state. In inactive bovine rhodopsin, the only GPCR for which structures had previously been determined (9, 10, 11), Arg^{3.50}, part of the highly conserved (D/E)RY motif in helix 3, forms a salt bridge with the conserved Glu^{6.30} in helix 6; Arg^{3.50} binds simultaneously to the adjacent residue in helix 3, Glu^{3.49}. (Superscripts refer to Ballesteros–Weinstein residue numbering* (12).) This salt bridge

network has been dubbed the “ionic lock” (13). Upon activation of rhodopsin, the intracellular ends of helices 3 and 6 move apart, breaking the Arg^{3.50}/Glu^{6.30} contact (14–17). A variety of biochemical evidence has suggested that the homologous residues in many other GPCRs, including the β -adrenergic receptors, also form an ionic lock in the inactive state (13, 18–21). Indeed, the term “ionic lock” was originally coined in a study of β_2 AR to describe the interaction of Arg-131^{3.50} with Glu-268^{6.30} and Asp-130^{3.49} (13). This interaction was believed to stabilize the inactive state, and its disruption was believed to be one of the critical events in the activation process (13, 21).

β_2 AR has been crystallized in complex with the partial inverse agonists carazolol and timolol (1–4); these structures should thus represent a nearly inactive state of the receptor. Although mostly similar to the structures of inactive rhodopsin, the β_2 AR structures lack the salt bridge between Arg-131^{3.50} and Glu-268^{6.30}, and the intracellular ends of helices 3 and 6 are substantially farther apart than in rhodopsin (Fig. 1 *A*, *B*, and *D*). The distance between the C $_{\alpha}$ atoms of Arg^{3.50} and Glu^{6.30} (which we refer to as the C $_{\alpha}$ –C $_{\alpha}$ distance) and the minimum distance between a guanidinium nitrogen atom of Arg^{3.50} and a carboxylate oxygen atom of Glu^{6.30} (the N–O distance) are listed in Table 1 for several GPCR crystal structures. In the adrenergic receptor structures, both distances are notably larger than in inactive rhodopsin.

The unexpected observation of a broken ionic lock in crystal structures of inactive β_2 AR has engendered substantial speculation regarding the reasons for the broken lock and possible implications for signaling by non-rhodopsin GPCRs (1, 3, 22–25). The broken lock might be a consequence of the techniques used to stabilize β_2 AR for crystallization, which involved either fusion with T4 lysozyme (T4L) or cocrystallization with an antibody Fab fragment. This is unlikely to be the full explanation, however, because a recent crystal structure of the β_1 -adrenergic receptor (β_1 AR), which was stabilized in a very different manner, also had a broken ionic lock (23). Additional hypotheses that have been proposed include: (i) β_2 AR may not form an ionic lock at all in the unliganded (apo) or partial-inverse-agonist-bound forms, perhaps reflecting the basal activity of these forms (3, 23); (ii) the lock may be formed in the apo receptor but break upon binding of carazolol or timolol, perhaps reflecting the ability of certain (but not all) partial inverse agonists to induce signaling through non-G-protein-dependent pathways

Author contributions: R.O.D., D.H.A., D.W.B., M.Ø.J., and D.E.S. designed research; R.O.D., D.H.A., and D.W.B. performed research; R.O.D., D.H.A., M.Ø.J., and S.P. analyzed data; and R.O.D., D.H.A., D.W.B., and D.E.S. wrote the paper.

The authors declare no conflict of interest.

This article is a PNAS Direct Submission.

Freely available online through the PNAS open access option.

¹R.O.D. and D.H.A. contributed equally to this work.

²To whom correspondence should be addressed. E-mail: David.Shaw@DEShawResearch.com.

*In Ballesteros–Weinstein numbering, x.50 denotes the most-conserved residue in helix x across the class A (rhodopsin-family) GPCRs. Other residues in that helix are numbered relative to this most-conserved residue.

This article contains supporting information online at www.pnas.org/cgi/content/full/0811065106/DCSupplemental.

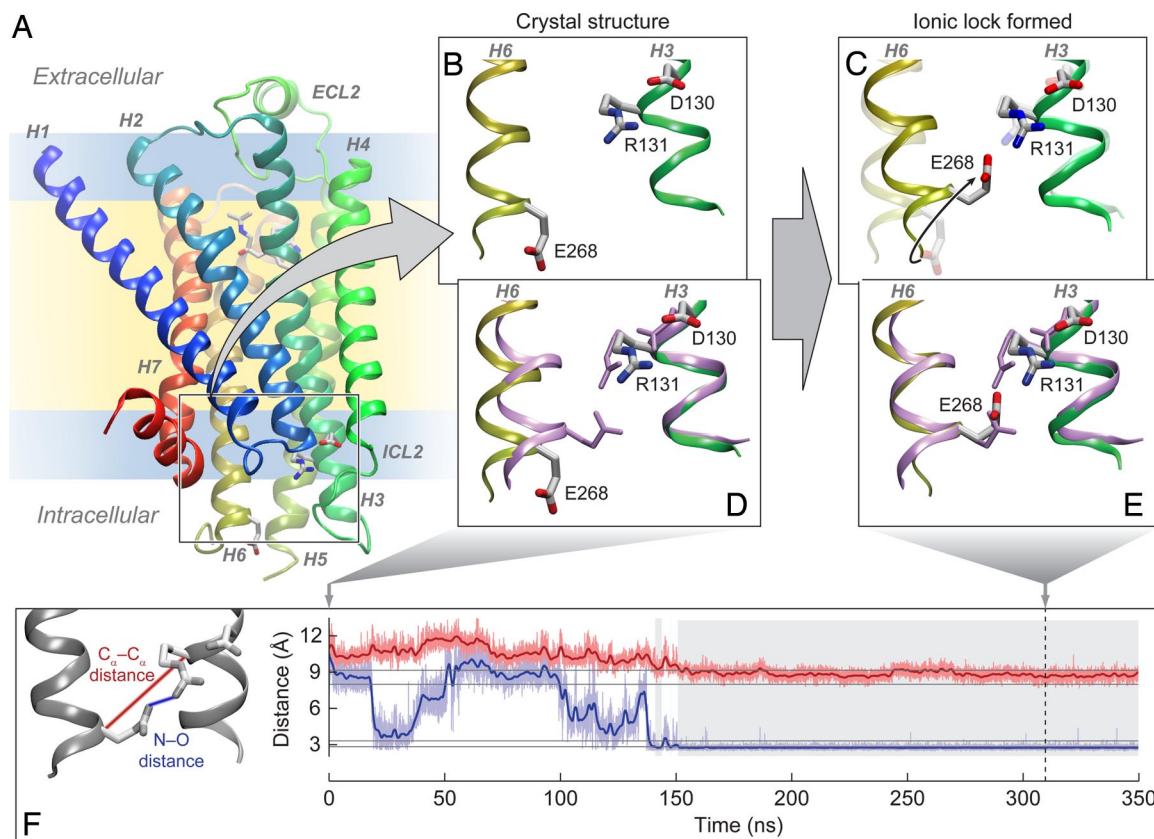


Fig. 1. Ionic lock formation in β_2 AR is accompanied by transition to an inactive-rhodopsin-like conformation. (A) The β_2 AR crystal structure (2RH1). (B) Close-up of the intracellular ends of helices 3 and 6 in the crystal structure showing the broken ionic lock. (C) A representative simulated conformation with the ionic lock formed. (D and E) Same conformations as shown in B and C with the homologous residues of inactive rhodopsin (1GZM; purple) superimposed. (F) C_α - C_α (light red) and N-O (light blue) distance time series for simulation c of Table 2, with smoothed versions included in dark red and blue; gray shading indicates when the smoothed C_α - C_α distance is < 9.5 Å. The upper pair of gray horizontal lines indicates C_α - C_α distances of inactive rhodopsin structures 1U19 and 1L9H, and the lower pair indicates the corresponding N-O distances.

(22, 24); or (iii) the inactive state may exist in an equilibrium between conformations with the ionic lock formed and broken (1, 25), in which case the crystal structures may or may not represent the conformation predominant in native membranes.

To distinguish among these hypotheses, we performed all-atom MD simulations of various β_2 AR constructs in a lipid bilayer, both with and without bound carazolol (Table 2). Using recently developed algorithms for high-speed, parallel MD (26, 27), we were able to simulate the dynamics of β_2 AR over a total of >10 μ s, including several individual MD trajectories longer than 1 μ s. MD simulations have been used to characterize the dynamics of both rhodopsin (28–32) and β_2 AR (33, 34); earlier studies of β_2 AR used shorter simulations and focused largely on effects of ligand binding.

In simulations of wild-type-like constructs, we found that the ionic lock consistently formed within the first several hundred nanoseconds, causing the intracellular ends of helices 3 and 6 to approach one another and adopt a local structure strongly resembling that of inactive rhodopsin. Conformations with an intact ionic lock predominated, but they did interconvert with conformations in which the lock was broken. The equilibrium favored ionic lock formation regardless of whether β_2 AR was in its apo state or bound to carazolol, and whether the crystallographic T4L fusion partner was simply removed or replaced by a reconstructed loop. In simulations of several constitutively active mutants and of the β_2 AR-T4L fusion construct, the equilibrium shifted toward conformations with the ionic lock broken and helices 3 and 6 farther apart. Our results thus suggest that an intact ionic lock is not a require-

ment for an inactive state of β_2 AR, but rather that the wild-type receptor in the inactive state frequently adopts conformations with the ionic lock formed, in accord with biochemical observations indicating that the ionic lock stabilizes the inactive state (13, 21).

Beyond the ionic lock, we observed formation of structural motifs seen in crystal structures of other GPCRs, including a helix in intracellular loop 2. Our findings may provide a more comprehensive view of the inactive state of the β -adrenergic receptors, suggesting that the dynamic conformational ensembles of different GPCRs might be more similar than their static crystal structures would suggest.

Results and Discussion

We performed 9 explicit-solvent MD simulations of β_2 AR embedded in a hydrated lipid bilayer (Table 2), ranging in length from 0.5 μ s to 2.0 μ s. Each simulation began with a protein conformation based on the 2.4-Å resolution crystal structure of Cherezov et al. (2) (PDB entry 2RH1). Throughout each simulation, the overall protein conformation remained close to the crystal structure (Table S1), and the ligand-binding pocket and adjacent cavities remained hydrated at a low, approximately constant level (Fig. S1).

β_2 AR contains a highly flexible 43-residue loop between helices 5 and 6 (intracellular loop 3, or ICL3). To obtain well-diffracting crystals, Kobilka and colleagues stabilized β_2 AR by replacing 32 residues of ICL3 with T4L (2, 3). ICL3 links 2 domains which, when expressed from separate plasmids, self-assemble to form a functional receptor (35). These domains have been suggested to asso-

Table 1. Comparison of ionic lock conformations in GPCR crystal structures

PDB ID	Protein	C _α -C _α , Å	N-O, Å	Notes
2RH1	β ₂ AR	11.2	9.9	T4L fusion
3D4S	β ₂ AR	11.0	9.1	T4L fusion
2R4R	β ₂ AR	11.1	6.4	Fab complex
2VT4	β ₁ AR	11.0	6.1	Thermostabilized
1U19	Rhodopsin	9.1	3.2	Inactive
1L9H	Rhodopsin	8.0	2.8	Inactive
1GZM	Rhodopsin	8.7	3.0	Inactive
3DQB	Opsin	14.2	15.3	Active

In the β-adrenergic receptor structures, the C_α-C_α distance (between the C_α atoms of Arg^{3.50} and Glu^{6.30}) and the N-O distance (the minimum distance between a guanidinium nitrogen atom of Arg^{3.50} and a carboxylate oxygen atom of Glu^{6.30}) are both substantially greater than in inactive rhodopsin, but substantially less than in active opsin. The adrenergic receptor structures were all determined with bound partial inverse agonists or antagonists (carazolol for 2RH1 and 2R4R, timolol for 3D4S, and cyanopindolol for 2VT4). Carazolol reduces the basal activity of unliganded β₂AR 2-fold (1).

ciate via a relatively dynamic interface (3). Because the rigidity of T4L may affect the relative position and dynamics of these domains, we eliminated it from most of our simulations. Experimentally, removal of the bulk of ICL3 by partial tryptic digest does not appear to affect receptor function (36). In most cases, we simply removed the T4L, leaving the residues that attach to it unconnected. We refer to the resulting protein as the clipped construct, or β₂AR-clipped. For comparison, we performed a simulation in which we replaced T4L with a model of ICL3 (the β₂AR-ICL3 construct), and a simulation of the intact β₂AR-T4L fusion protein.

Ionic Lock Forms Reproducibly in Carazolol-Bound and Apo β₂AR-Clipped. In each of 4 simulations of β₂AR-clipped with bound carazolol (Table 2, simulations *a-d*), β₂AR adopted a conformation

Table 2. Properties of each β₂AR MD simulation

Simulation	Construct	Ligand	Length, ns	C _α -C _α < 9.5 Å, %
Four replicates with different initial conditions				
<i>a</i>	β ₂ AR-clipped	Carazolol	2,004	90
<i>b</i>	β ₂ AR-clipped	Carazolol	510	96
<i>c</i>	β ₂ AR-clipped	Carazolol	522	83
<i>d</i>	β ₂ AR-clipped	Carazolol	770	96
Variants of simulated system				
<i>e</i>	β ₂ AR-clipped	—	1,031	91
<i>f</i>	β ₂ AR-ICL3	Carazolol	1,094	92
<i>g</i>	β ₂ AR-T4L	Carazolol	1,020	41
<i>h</i>	β ₂ AR-clipped/E268A	Carazolol	1,023	20
<i>i</i>	β ₂ AR-clipped/D130N	Carazolol	1,137	53

We used PDB entry 2RH1 as the basis for all simulations. Simulated constructs include β₂AR-T4L (the crystallized T4 lysozyme fusion protein), β₂AR-clipped (in which T4L was removed, leaving 282 residues), and β₂AR-ICL3 (in which T4L was replaced by a model of intracellular loop 3). The last column represents the percentage of time during which the C_α-C_α distance was <9.5 Å, beginning at 150 ns.

with the ionic lock formed and the intracellular ends of helices 3 and 6 closer to each other (Fig. 1). Over a period of 30–165 ns, the C_α-C_α and N-O distances shortened from those of the 2.4-Å resolution β₂AR crystal structure (11.2 Å and 9.9 Å, respectively) to distances typical of inactive rhodopsin structures (≈8.8 Å and ≈2.8 Å) (Fig. 2*a* and Fig. S2*a-d*). As shown in Fig. 1, Arg-131^{3.50} formed salt bridges with both Glu-268^{6.30} and Asp-130^{3.49} that mirror the interactions of Arg^{3.50} with Glu^{6.30} and Glu^{3.49} in inactive rhodopsin. Relative to the β₂AR crystal structure, the intracellular end of helix 6 moved toward helix 3, kinking slightly at Gly-276^{6.38}. Occasionally, helix 6 straightened without breaking the ionic lock, causing helix 3 to bend inward.

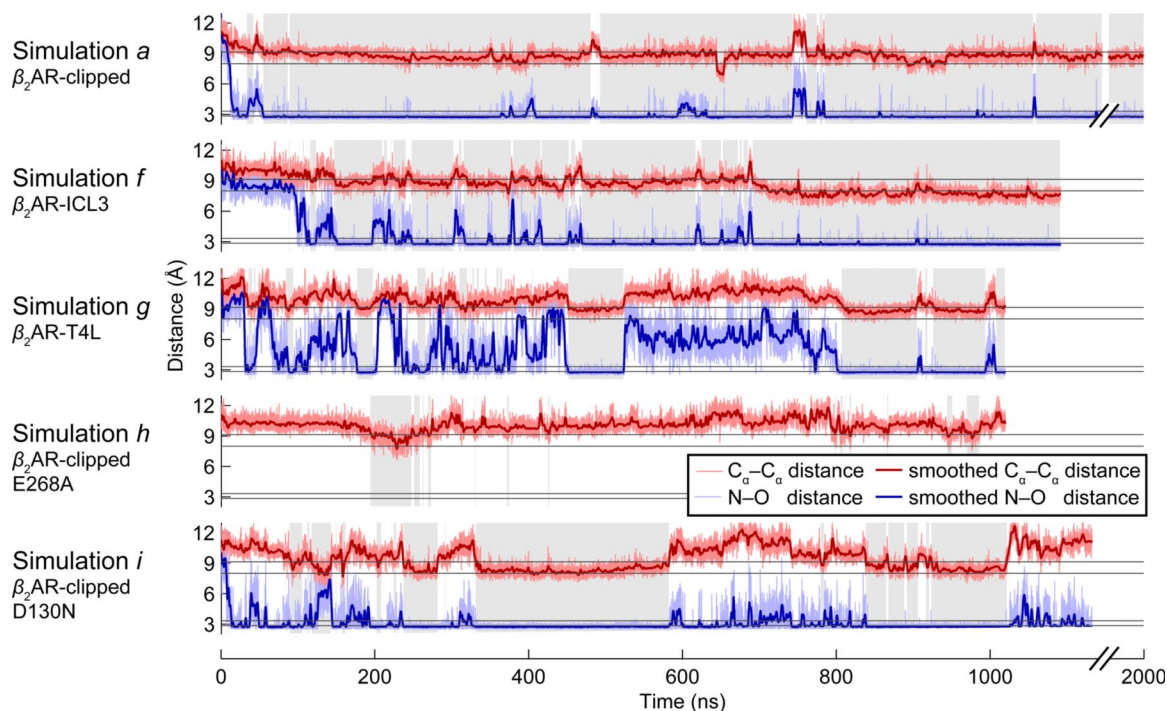


Fig. 2. Ionic lock closure depends on the form of β₂AR. C_α-C_α and N-O distance time series for 5 simulations (simulations *a* and *f-i* in Table 2), colored as in Fig. 1*F*. Simulations of β₂AR-clipped and β₂AR-ICL3 (simulations *a* and *f*) exhibited C_α-C_α and N-O distances comparable to those of inactive rhodopsin most of the time; helices 3 and 6 occasionally moved apart during transient breakage of the ionic lock. By contrast, the crystallographic construct β₂AR-T4L (simulation *g*), and the constitutively active mutants E268A (simulation *h*) and D130N (simulation *i*), exhibited a substantially greater interhelical distance and a broken ionic lock for a larger fraction of the time.

Conformations with the ionic lock formed and the helices close together predominated in each of these simulations. The N-O distance time series of Fig. 2*a* and Fig. S2*a-d* show that the ionic lock frequently broke and then reformed within a few nanoseconds, usually without a corresponding increase in the distance between the backbones of helices 3 and 6 (as measured by the C $_{\alpha}$ -C $_{\alpha}$ distance, which remained close to 9 Å). Every few hundred nanoseconds, however, the helices moved apart upon ionic lock breakage, with the C $_{\alpha}$ -C $_{\alpha}$ distance increasing to \approx 11 Å; this conformational state, which was similar to that of the β_2 AR crystal structures, typically persisted for tens of nanoseconds. The C $_{\alpha}$ -C $_{\alpha}$ distance was $<$ 9.5 Å 91% of the time, on average, in simulations *a-d*, excluding the first 150 ns of each. This observed occupancy implies that the state with the helices together has a free energy \approx 1.4 kcal/mol lower than the state with the helices apart (see *SI Text* for additional detail).

A simulation of β_2 AR-clipped without any ligand (*e* in Table 2 and Fig. S2) behaved similarly with respect to both the ionic lock and the positions of helices 3 and 6. Removal of the partial inverse agonist carazolol did not appear to weaken the lock; this observation likely reflects the fact that entry to the active state involves additional motions beyond lock breakage, although our microsecond-timescale simulations may not suffice to capture modest changes in the conformational distribution. Our results suggest that inactive β_2 AR, whether ligand-free or inverse-agonist-bound, exists in equilibrium between a conformation in which the ionic lock is formed and a conformation in which it is broken, and that conformations with the ionic lock formed may predominate.

Ionic Lock Forms in β_2 AR-ICL3 but Not in β_2 AR-T4L. The ionic lock also formed and remained intact for most of the 1.1 μ s simulation of β_2 AR-ICL3 (*f* in Table 2 and Fig. 2); in this construct, the native intracellular loop 3 sequence, initially in an unfolded conformation, linked helices 5 and 6. During the first 700 ns, the loop was very mobile, rapidly transitioning through a wide range of orientations and conformations (Fig. S3). The ionic lock broke several times more frequently than in simulations of β_2 AR-clipped, apparently because the motion of ICL3 sometimes pulled the intracellular end of helix 6 away from helix 3. Over the last 400 ns, however, ICL3 assumed a relatively stable folded conformation, forming 2 short α -helices (residues 235–239 and 252–259) and extending helix 6 by 3 residues (Fig. S3*c*). The short α -helices packed against the ends of helices 5 and 6, causing the end of helix 6 to kink toward helix 3, which stabilized the ionic lock. This structure adopted by ICL3 may well unfold in longer simulations, particularly given that the sequence of ICL3 shows evidence of intrinsic disorder (37), but these observations are interesting nonetheless, because ICL3 is believed to be a determinant of G protein specificity (23, 38).

A simulation of β_2 AR-T4L (*g* in Table 2 and Fig. 2) behaved very differently. Although the ionic lock formed occasionally, it was usually broken, with the C $_{\alpha}$ -C $_{\alpha}$ distance $<$ 9.5 Å only 41% of the time. In the crystal structure, Glu-268^{6,30} forms a salt bridge with Arg-8 of T4L. This salt bridge was broken for most of the β_2 AR-T4L simulation and thus did not appear to prevent ionic lock formation. Instead, the rigidity of T4L appears to prevent helix 6 from approaching helix 3.

Mutations That Disrupt the Ionic Lock Increase the Separation of Helices 3 and 6. We simulated 2 β_2 AR mutants, Glu-268^{6,30}Ala and Asp-130^{3,49}Asn, that have been shown experimentally to increase ligand-independent activity (13). This constitutive activity was attributed to disruption of the ionic lock, which was assumed to be formed in the inactive state (13). In simulations of mutated β_2 AR-clipped with bound carazolol (*h* and *i* in Table 2 and Fig. 2), each mutation disrupted the lock and led to an increase in the distance between the intracellular ends of helices 3 and 6: The C $_{\alpha}$ -C $_{\alpha}$ distance fell below 9.5 Å only 20% (Glu-268^{6,30}Ala) and 53% (Asp-130^{3,49}Asn) of the time, as opposed to $>$ 90% of the time in the absence of these mutations.

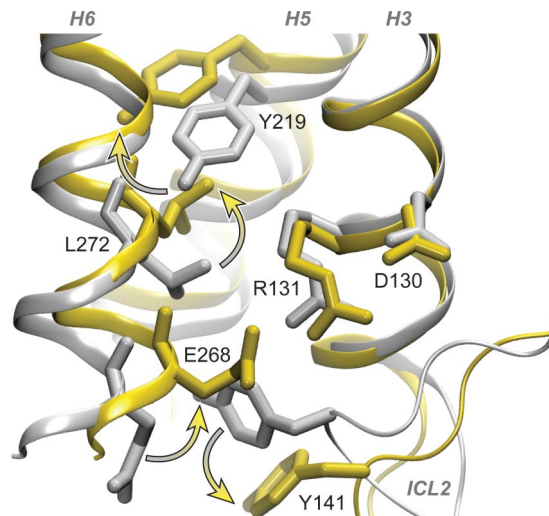


Fig. 3. Side chain rearrangements at the interface of helices 3, 5, and 6 enable stable ionic lock formation. In the crystal structure (gray), Y219 is located between helices 3 and 6 and contacts R131. To adopt an ionic-lock-formed conformation (yellow), Y219 rotated to the lipid-exposed side of helix 6 and L272 rotated from *gauche*⁻ to *trans*, enabling the end of helix 6 to move toward helix 3 and E268 to approach R131. Independently, Y141 rotated out from between R131 and E268 to enable formation of the R131–E268 contact.

The Glu-268^{6,30}Ala mutation eliminated the salt bridge with Arg-131^{3,50} and thereby directly reduced the propensity of helices 3 and 6 to approach one another. The Asp-130^{3,49}Asn mutation, however, did not eliminate the Arg-131^{3,50}–Glu-268^{6,30} salt bridge; one might even have imagined it to strengthen that salt bridge by eliminating the other negatively charged partner to the positive arginine. This mutation, however, allowed the arginine side chain to separate more easily from residue 130^{3,49} and extend toward helix 6, such that helices 3 and 6 could move farther apart while maintaining the Arg-131^{3,50}–Glu-268^{6,30} salt bridge. Perhaps more importantly, the lack of preorganization of Arg-131^{3,50} by Asp-130^{3,49} increased the entropic cost of forming the Arg-131^{3,50}–Glu-268^{6,30} salt bridge, causing it to be broken more of the time.

Other Side Chain Conformational Changes Precede Ionic Lock Formation. In the β_2 AR crystal structures, Tyr-141 of intracellular loop 2 (ICL2) is positioned between Arg-131^{3,50} and Glu-268^{6,30}, such that formation of the ionic lock would be impossible without Tyr-141 moving aside. In our simulations, Tyr-141 moved toward the intracellular space within 100 ns (Fig. 3) and never returned to its initial position, even when the ionic lock transiently broke.

In addition, we consistently observed a rearrangement of conserved hydrophobic residues at the interface of helices 3, 5, and 6 that permitted stable ionic lock formation. As shown in Fig. 3, the Tyr-219^{5,58} side chain rotated from between helices 3 and 6 to the lipid-exposed side of helix 6, and Leu-272^{6,34} rotated from *gauche*⁻ to *trans*, allowing the backbone of Glu-268^{6,30} to approach Arg-131^{3,50} and the salt bridge to form.

In inactive rhodopsin (9–11), the Tyr^{5,58} side chain resides on the lipid-exposed side of helix 6, enabling tight packing between helices 3 and 6, whereas in active opsin (17), it is wedged between helices 3 and 6 in a gap opened by outward movement of helix 6. In this latter conformation, Tyr^{5,58} forms a hydrogen bond with Arg^{3,50}, stabilizing the interaction of Arg^{3,50} with the G protein (17). In the Fab-bound β_2 AR structure (1), as in inactive rhodopsin, Tyr^{5,58} is lipid-exposed, whereas in β_2 AR-T4L (which has constitutively-active-like properties), Tyr^{5,58} lies between helices 3 and 6. Taken together, our simulation results and the crystal structures suggest that the rotation of Tyr^{5,58} and rearrangement of neighboring conserved residues may be a key step along the activation pathway of β_2 AR.

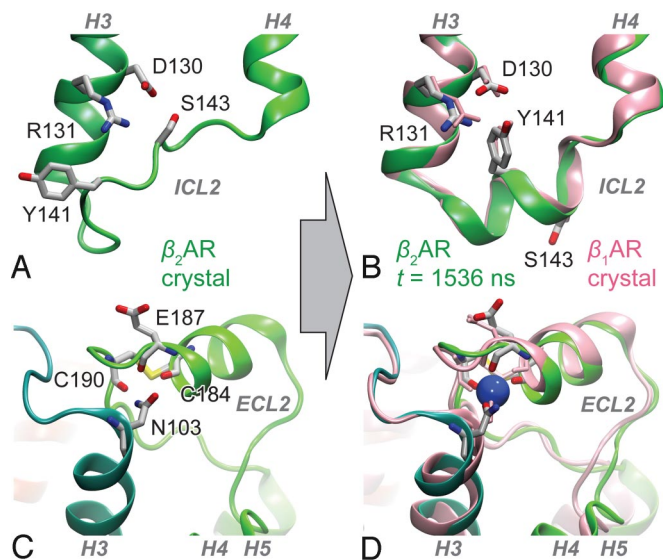


Fig. 4. Structural elements homologous to β_1 AR form spontaneously during simulation of β_2 AR. Selected side chains and adjoining helices of intracellular loop 2 (ICL2) (A) and extracellular loop 2 (ECL2) (C) of the β_2 AR crystal structure. Representative helical conformation of ICL2 adopted during simulation *a*, superimposed on the corresponding region of the β_1 AR structure (pink) (B), and of ECL2 with bound sodium ion, superimposed on the sodium binding site of β_1 AR (D).

Phe-264^{6,26}, which exhibits different conformations in the β_2 AR-T4L and β_2 AR/Fab structures, has been hypothesized to stabilize inactive wild-type β_2 AR through interactions with helix 5, helix 6, and ICL2 (3). In our β_2 AR-T4L simulation, Phe-264^{6,26} remained close to its crystallographic conformation. In simulations of β_2 AR-clipped and β_2 AR-ICL3, Phe-264^{6,26} adopted a conformation different from either crystal structure; helix 6 extended to include Phe-264^{6,26}, whose side chain usually pointed away from helix 5, frequently into the cytoplasm.

β_2 AR Loops Adopt Secondary Structure, Matching β_1 AR. We observed the spontaneous formation of several secondary structural elements in both extracellular and intracellular loops, in addition to the folding of ICL3 mentioned above. After $\approx 1 \mu\text{s}$ of simulation *a*, ICL2, which exhibited a random coil conformation in the β_2 AR crystal structures, folded into an α -helix essentially identical to that observed in the crystal structure of β_1 AR (Fig. 4 A and B). Based on their structural results for β_1 AR, Warne et al. (23) proposed that such a helix also exists in the inactive state of β_2 AR, noting that the ICL2 sequence is highly conserved between β_1 AR and β_2 AR, but that such a helix could not be accommodated in existing β_2 AR structures because of crystal lattice contacts. In the β_2 AR structures, Tyr-141 interacts with the ionic lock residues Arg-131^{3,50} and Glu-268^{6,30}. Once ICL2 folded in our simulation, Tyr-141 and Asp-130^{3,49} formed a hydrogen bond, as do the homologous Tyr-149 and Asp-138^{3,49} in the β_1 AR structure. The ICL2 α -helix and the Tyr-141–Asp-130^{3,49} hydrogen bond remained stable for the remaining $\approx 1 \mu\text{s}$ of simulation. These conformational changes may have implications for activation and G protein interaction (see *Concluding Remarks*).

We also observed that residues Cys-184, Glu-187, and Cys-190 of extracellular loop 2 (ECL2), and Asn-103^{3,22}, form a cation binding site; this site was occupied by a sodium ion over half the time, even though our simulations were not initiated with an ion at that site (Fig. 4 C and D). A sodium ion was bound at the same site in the β_1 AR structure (23). No such bound ion was reported in the β_2 AR structures, but we found a significant peak ($0.16 e^-/\text{\AA}^3$) at the site

on reexamination of β_2 AR-T4L (PDB entry 2RH1) difference electron density maps.

Simulation Results Match Biochemical Observations. Our simulations, which suggest that inactive β_2 AR frequently adopts conformations with the ionic lock formed, are consistent with a significant body of biochemical data on β_2 AR and other rhodopsin-family GPCRs.

By incorporating fluorophores into the intracellular ends of helices 3 and 6, for example, Kobilka and colleagues demonstrated that, in ligand-free β_2 AR, close contact of the fluorophores was prevented, which they interpreted as intersection of the Arg-131^{3,50}–Glu-268^{6,30} salt bridge (21). Agonist binding led to increased fluorescence quenching (shorter interfluorophore distance), presumably by breaking this salt bridge.

Mutational studies have shown that neutralization of either Glu-268^{6,30} or Asp-130^{3,49} in β_2 AR, and of homologous residues in other rhodopsin-family GPCRs, leads to increased agonist-dependent and -independent activation (13, 18–20, 39, 40). These β_2 AR mutants also show increased agonist affinity and increased accessibility of Cys-285^{6,47} to water (13), consistent with an increased propensity to assume an active state. Although our simulations are too short to observe activation, which takes place on the millisecond timescale (41), they clearly indicate that mutation of either Glu-268^{6,30} or Asp-130^{3,49} weakens the attractive interaction between helices 3 and 6 that stabilizes the inactive state.

Finally, our results suggest that, in β_2 AR-T4L, the T4L tends to keep helices 3 and 6 apart and the ionic lock broken, in accord with the observation that the fusion protein has certain properties characteristic of a constitutively active mutant (3). This explanation leaves open the question of why the β_2 AR/Fab complex and β_1 AR structures also exhibit a broken ionic lock. A number of explanations are plausible. First, all of these structures possess an artificially constrained ICL3 (by T4L fusion, Fab binding, or loop truncation); perhaps the inactive state conformational equilibrium is sensitive to these constraints. Second, the act of crystallization, through altered lipid mechanical and electrostatic properties, effects of specific reagents, or the constraints of lattice packing, may conspire to shift conformational equilibria of proteins in general and GPCRs in particular (42, 43). The relative occupancies estimated by our simulations may be biased by imperfect force fields, so we cannot rule out the possibility that the ionic lock may be predominantly broken in native β_2 AR and that other molecular mechanisms account for the biochemical data discussed above.

Concluding Remarks. Previous experimental work has indicated that GPCRs adopt multiple functionally relevant conformations within their active and inactive states (7, 8). We used microsecond-timescale MD simulations to characterize the inactive β_2 AR conformational ensemble, focusing on the biochemically defined ionic lock that proved to be unexpectedly broken in the recent β_2 AR and β_1 AR crystal structures. In our simulations, inactive β_2 AR alternates between a major conformation, with the lock formed and helices 3 and 6 close together, and a minor conformation, with the lock broken and helices separated. Certain constitutively activating mutations or replacement of ICL3 by T4L shift β_2 AR toward the lock-broken, separated-helices conformation, presumably closer to the active state.

An initially puzzling feature of our simulations was that the Glu-268^{6,30} Ala mutant exhibited greater separation of helices 3 and 6 than did Asp-130^{3,49} Asn, whereas experimentally Asp-130^{3,49} Asn exhibits greater constitutive activity (13). Very recently, the structure of activated opsin (17) revealed a second role for Arg^{3,50} beyond ionic lock formation: It binds to G_α in the active state. On this basis (17), we suggest that the β_2 AR Asp-130^{3,49} Asn mutation, by affording Arg-131^{3,50} increased conformational freedom, facilitates engagement of G_α by Arg-131^{3,50}. We speculate that this dual role explains how Arg^{3,50} mutations that increase activity in some rhodopsin-family GPCRs can decrease activity in others (39); any

particular Arg^{3,50} mutation alters the balance between interhelix stability and productive G_α engagement, in a manner that depends on the specific GPCR/G_α pair in question.

We also observed the formation of several structural motifs, including an α -helix in ICL2—absent from the β_2 AR crystal structures but present in β_1 AR—which may modulate G_α binding. The results obtained here with β_2 AR may be pertinent to many rhodopsin-family GPCRs, as suggested by the recent A_{2A} adenosine receptor (A_{2A}AR) structure (44), which possesses a helix in ICL2 as well. Additionally, A_{2A}AR, which like β_2 AR was crystallized as a T4L fusion protein, also exhibited a broken ionic lock and had Tyr^{5,58} positioned between helices 3 and 6, again suggesting that the T4L biases the inactive conformational equilibrium in the direction of the active state.

Beyond a more comprehensive description of the inactive state, our observations provide clues to changes that may occur upon receptor activation. First, because the ionic lock appears to be frequently intact in the inactive state, lock breakage and separation of helices 3 and 6 may be a step toward activation. Second, because ICL2 is known to play a role in G_α binding and activation (23, 38), we speculate that during activation protonation of Asp^{3,49} and attendant weakening of the Tyr-141–Asp^{3,49} hydrogen bond may

disorder the ICL2 helix, facilitating the formation of contacts with G_α. Third, it was recently suggested that the basal activity profile among β_1 AR, β_2 AR and A_{2A}AR correlates with the presence of the helix in ICL2 and the Tyr-141–Asp^{3,49} hydrogen bond (44). Our observation that β_2 AR, like β_1 AR and A_{2A}AR, can form a stable ICL2 helix suggests instead that the basis for differential basal activity among these receptors either involves differences in ICL2 helix stability or lies elsewhere.

Methods

We used the CHARMM27 force field (45) with the CMAP backbone energy correction (46) for all simulations. This and earlier versions of the CHARMM force field have been used in previous studies of both rhodopsin (28, 30–32) and β_2 AR (33, 34), and in studies of salt bridge formation in various proteins (47, 48). N-terminal residues 1–28 and C-terminal residues 343–413 were omitted from all simulations, because they were truncated or not resolved in the crystal structure. All simulations also included a glutamate at position 187, reflecting an Asn187Glu mutation made in the crystallization construct to eliminate a glycosylation site. Molecular graphics were produced using VMD (49). Further details are provided in *SI Text*.

ACKNOWLEDGMENTS. We thank Michael Eastwood, Justin Gullingsrud, Kresten Lindorff-Larsen, Paul Maragakis, and Kim Palmo for helpful discussions, and Rebecca Kastleman for editorial assistance.

- Rasmussen SGF, et al. (2007) Crystal structure of the human β_2 adrenergic G-protein-coupled receptor. *Nature* 450:383–387.
- Cherezov V, et al. (2007) High-resolution crystal structure of an engineered human β_2 -adrenergic G protein-coupled receptor. *Science* 318:1258–1265.
- Rosenbaum DR, et al. (2007) GPCR engineering yields high-resolution structural insights into β_2 -adrenergic receptor function. *Science* 318:1266–1273.
- Hanson MA, et al. (2008) A specific cholesterol binding site is established by the 2.8 Å structure of the human β_2 -adrenergic receptor. *Structure* 16:897–905.
- Lundstrom K (2006) Latest development in drug discovery on G protein-coupled receptors. *Curr Protein Pept Sci* 7:465–470.
- Lefkowitz RJ (2000) The superfamily of heptahelical receptors. *Nat Cell Biol* 2:E133–E136.
- Galandrin S, Bouvier M (2006) Distinct signaling profiles of β_1 and β_2 adrenergic receptor ligands toward adenylyl cyclase and mitogen-activated protein kinase reveals the pluridimensionality of efficacy. *Mol Pharmacol* 70:1575–1584.
- Kobilka BK, Deupi X (2007) Conformational complexity of G-protein-coupled receptors. *Trends Pharmacol Sci* 28:397–406.
- Palczewski K, et al. (2000) Crystal structure of rhodopsin: A G protein-coupled receptor. *Science* 289:739–745.
- Okada T, et al. (2004) The retinal conformation and its environment in rhodopsin in light of a new 2.2 Å crystal structure. *J Mol Biol* 342:571–583.
- Li J, Edwards PC, Burghammer M, Villa C, Schertler GFX (2004) Structure of bovine rhodopsin in a trigonal crystal form. *J Mol Biol* 343:1409–1438.
- Ballesteros JA, Weinstein H (1995) Integrated methods for the construction of three dimensional models and computational probing of structure function relations in G protein-coupled receptors. *Methods Neurosci* 25:366–428.
- Ballesteros JA, et al. (2001) Activation of the β_2 -adrenergic receptor involves disruption of an ionic lock between the cytoplasmic ends of transmembrane segments 3 and 6. *J Biol Chem* 276:29171–29177.
- Sheikh SP, Zvyaga TA, Lichtarge O, Sakmar TP, Bourne HR (1996) Rhodopsin activation blocked by metal-ion-binding sites linking transmembrane helices C and F. *Nature* 383:347–350.
- Farrens DL, Altenbach C, Yang K, Hubbell WL, Khorana HG (1996) Requirement of rigid-body motion of transmembrane helices for light activation of rhodopsin. *Science* 274:768–770.
- Altenbach C, Kusnetzow AK, Ernst OP, Hofmann KP, Hubbell WL (2008) High-resolution distance mapping in rhodopsin reveals the pattern of helix movement due to activation. *Proc Natl Acad Sci USA* 105:7439–7444.
- Scheerer P, et al. (2008) Crystal structure of opsin in its G-protein-interacting conformation. *Nature* 455:497–502.
- Greasley PJ, Fanelli F, Rossier O, Abuin L, Cotecchia S (2002) Mutagenesis and modelling of the α_{1B} -adrenergic receptor highlight the role of the helix 3/helix 6 interface in receptor activation. *Mol Pharmacol* 61:1025–1032.
- Angelova K, Fanelli F, Puett D (2002) A model for constitutive lutropin receptor activation based on molecular simulation and engineered mutations in transmembrane helices 6 and 7. *J Biol Chem* 277:32202–32213.
- Shapiro DA, Kristiansen K, Weiner DM, Kroeze WK, Roth BL (2002) Evidence for a model of agonist-induced activation of 5-hydroxytryptamine 2A serotonin receptors that involves the disruption of a strong ionic interaction between helices 3 and 6. *J Biol Chem* 277:11441–11449.
- Yao X, et al. (2006) Coupling ligand structure to specific conformational switches in the β_2 -adrenoceptor. *Nat Chem Biol* 2:417–422.
- Audet M, Bouvier M (2008) Insights into signaling from the β_2 -adrenergic receptor structure. *Nat Chem Biol* 4:397–403.
- Warne T, et al. (2008) Structure of a β_1 -adrenergic G-protein-coupled receptor. *Nature* 454:486–491.
- Lefkowitz RJ, Sun JP, Shukla AK (2008) A crystal clear view of the β_2 -adrenergic receptor. *Nat Biotechnol* 26:189–191.
- Ranganathan R (2007) Signaling across the cell membrane. *Science* 318:1253–1254.
- Bowers KJ, et al. (2006) Scalable algorithms for molecular dynamics simulations on commodity clusters. *Proceedings of the 2006 ACM/IEEE Conference on Supercomputing (SC06)* (ACM Press, New York).
- Bowers KJ, Dror RO, Shaw DE (2006) The midpoint method for parallelization of particle simulations. *J Chem Phys* 124:184109.
- Saam J, Tajkhorshid E, Hayashi S, Schulten K (2002) Molecular dynamics investigation of primary photoinduced events in the activation of rhodopsin. *Biophys J* 83:3097–3112.
- Röhrlig UF, Guidoni L, Laio A, Frank I, Rothlisberger U (2004) A molecular spring for vision. *J Am Chem Soc* 126:15328–15329.
- Martinez-Mayorga K, Pitman MC, Grossfield A, Feller SE, Brown MF (2006) Retinal counterion switch mechanism in vision evaluated by molecular simulations. *J Am Chem Soc* 128:16502–16503.
- Grossfield A, Pitman MC, Feller SE, Soubias O, Gawrisch K (2008) Internal hydration increases during activation of the G-protein-coupled receptor rhodopsin. *J Mol Biol* 381:478–486.
- Tikhonova IG, et al. (2008) Atomistic insights into rhodopsin activation from a dynamic model. *J Am Chem Soc* 130:10141–10149.
- Spijker P, Vaidehi N, Freddolino PL, Hilbers PAJ, Goddard WA III (2006) Dynamic behavior of fully solvated β_2 -adrenergic receptor, embedded in the membrane with bound agonist or antagonist. *Proc Natl Acad Sci USA* 103:4882–4887.
- Huber T, Menon S, Sakmar TP (2008) Structural basis for ligand binding and specificity in adrenergic receptors: Implications for GPCR-targeted drug discovery. *Biochemistry* 47:11013–11023.
- Kobilka BK, et al. (1988) Chimeric α_2 - β_2 -adrenergic receptors: Delineation of domains involved in effector coupling and ligand binding specificity. *Science* 240:1310–1316.
- Rubenstein RC, Wong SK, Ross EM (1987) The hydrophobic tryptic core of the beta-adrenergic receptor retains Gs regulatory activity in response to agonists and thiols. *J Biol Chem* 262:16655–16662.
- Jaakola VP, Prilusky J, Sussman JL, Goldman A (2005) G protein-coupled receptors show unusual patterns of intrinsic unfolding. *Protein Eng Des Sel* 18:103–110.
- Ostrowski J, Kjelsberg MA, Caron MG, Lefkowitz RJ (1992) Mutagenesis of the β_2 -adrenergic receptor: How structure elucidates function. *Annu Rev Pharmacol Toxicol* 32:167–183.
- Rovati GE, Capra V, Neubig RR (2007) The highly conserved DRY motif of class A G protein-coupled receptors: Beyond the ground state. *Mol Pharmacol* 71:959–964.
- Vogel R, et al. (2008) Functional role of the “ionic lock”—an interhelical hydrogen bond network in family A heptahelical receptors. *J Mol Biol* 380:648–655.
- Vilardaga JP, Bünemann M, Krasel C, Castro M, Lohse MJ (2003) Measurement of the millisecond activation switch of G protein-coupled receptors in living. *Nat Biotechnol* 21:807–812.
- Wang Y, Botelho AV, Martinez GV, Brown MF (2002) Electrostatic properties of membrane lipids coupled to metarhodopsin II formation in visual transduction. *J Am Chem Soc* 124:7690–7701.
- Schwartz TW, Hubbell WL (2008) A moving story of receptors. *Nature* 455:473–474.
- Jaakola VP, et al. (2008) The 2.6 Å crystal structure of a human A2A adenosine receptor bound to an antagonist. *Science* 322:1211–1217.
- MacKerell AD, et al. (1998) All-atom empirical potential for molecular modeling and dynamics studies of proteins. *J Phys Chem B* 102:3586–3616.
- MacKerell AD, Feig M, Brooks CL III (2004) Extending the treatment of backbone energetics in protein force fields: Limitations of gas-phase quantum mechanics in reproducing protein conformational distributions in molecular dynamics simulations. *J Comp Chem* 25:1400–1415.
- Guidoni L, Torre V, Carloni P (1999) Potassium and sodium binding to the outer mouth of the K⁺ channel. *Biochemistry* 38:8599–8604.
- Yin Y, Jensen MO, Tajkhorshid E, Schulten K (2006) Sugar binding and protein conformational changes in lactose permease. *Biophys J* 91:3972–3985.
- Humphrey W, Dalke A, Schulten K (1996) VMD—Visual molecular dynamics. *J Mol Graphics* 14:33–38.